



Sustainable Industrial Wastewater Treatment and Antibacterial Activity using Environmental Friendly Ferrite Nanoparticles

M. SATHISH^{1,*}, V. SATHANA¹, A. VENKATESAN², S. DAVID AMALRAJ³, ANAND GASPAR³,
M. MARIA JULIE¹ and JAYABALAN JAYAPRAKASH⁴

¹Department of Physics, St. Joseph's College of Arts & Science (Autonomous), Cuddalore-607001, India

²Department of Mathematics, St. Joseph's College of Arts & Science (Autonomous), Cuddalore-607001, India

³Department of Chemistry, St. Joseph's College of Arts & Science (Autonomous), Cuddalore-607001, India

⁴Department of Microbiology, St. Joseph's College of Arts & Science (Autonomous), Cuddalore-607001, India

*Corresponding author: E-mail: sathishmary2013@gmail.com

Received: 9 November 2023;

Accepted: 29 December 2023;

Published online: 31 January 2024;

AJC-21525

A comparison studies of two unique bimetallic spinel ferrite nanoparticles synthesized by the sol-gel process, namely Co-NiFe₂O₄ and Cu-ZnFe₂O₄ were investigated. Various characterization approaches were utilized to examine the structural, morphological, magnetic and electrical characteristics of the nanoparticles. Both Co-NiFe₂O₄ and Cu-ZnFe₂O₄ nanoparticles formed single-phase spinel structures, according to X-ray diffraction (XRD) research whereas FTIR spectra provided information about the vibrational modes and chemical bonding within the nanoparticles confirmed the presence of desired metal-oxygen bonds chemical bonding within the nanoparticles. The UV-Vis spectroscopy revealed the optical absorption properties of the nanoparticles indicating the presence of energy bandgaps in the visible range. Scanning electron microscopy (SEM) images suggested the uniform and well-dispersed nanoparticles with average sizes in the nanoscale range. Vibrating sample magnetometry (VSM) measurements demonstrated that both Co-NiFe₂O₄ and Cu-ZnFe₂O₄ nanoparticles exhibited ferromagnetic behaviour at room temperature. The saturation magnetization values were found to be higher for Co-NiFe₂O₄ nanoparticles compared to Cu-ZnFe₂O₄ nanoparticles, suggesting the superior magnetic properties of the former. As a result, ferrites demonstrate promise in industrial wastewater treatment, facilitating efficient heavy metal removal and advanced organic pollutant degradation, contributing to a sustainable and effective solution. The antibacterial efficacy of synthesized bimetallic ferrite nanoparticles against *Salmonell typhi*, *Escherichia coli*, *Staphylococcus aureus*, *Bacillus cereus* proves that the synthesized ferrite nanoparticles possess a good antibacterial activity against the selected pathogens.

Keywords: Magnetic properties, Spinel structures, Ferromagnetic, Ferrites, Saturation magnetization, Antibacterial.

INTRODUCTION

Ferrite nanoparticles have become a new class of materials with intriguing characteristics and a wide range of uses [1-7]. These nanoparticles have a crystal lattice structure and are made up of oxygen and transition metal ions, usually iron [8]. Ferrite nanoparticles have a singular mix of magnetic, electrical and catalytic capabilities, which has sparked substantial study into the investigation of their potential in a variety of domains [9-11]. Compared to their bulk counterparts, ferrite nanoparticles have a number of benefits. Their smaller size, usually between 1 and 100 nm, induces quantum confinement effects and raises the surface-to-volume ratio, which improves their physical and

chemical characteristics [12-16]. Additionally, the size, content and morphology of these materials may be controlled during their synthesis, which enables the fine-tuning of their characteristics for particular uses [17-21]. Spinel ferrites, which have the general formula AB₂O₄ with differing transition metal ions for A and B, are the most prevalent variety of ferrite nanoparticles [22-25]. Nanoparticles made of Co-NiFe₂O₄ and Cu-ZnFe₂O₄ are examples of the spinel ferrites. Due to the spin interactions between the transition metal ions, these nanoparticles have an unusual magnetic behaviour and a cubic crystal structure.

Co-NiFe₂O₄ nanoparticles are composed of cobalt, nickel and iron ions. The combination of these transition metals in the crystal lattice results in enhanced the magnetic properties,

making them attractive for applications in magnetic storage, sensors and microwave absorption [26-29]. Co-NiFe₂O₄ is a notable compound categorized as a spinel ferrite, a class of mixed-metal oxide materials with a unique cubic crystal structure. This structure consists of oxygen ions arranged in a cubic close-packed manner, while metal ions occupy both octahedral and tetrahedral sites within the lattice. The ability to tune the composition and size of Co-NiFe₂O₄ nanoparticles allows for control over their magnetic response and enables their use in various technological advancements.

The Cu-ZnFe₂O₄ nanoparticles, on the other hand, consist of copper, zinc and iron ions. These nanoparticles exhibit interesting electrical and catalytic properties due to the presence of copper and zinc in the crystal structure [30-34]. The crystal structure of Cu-ZnFe₂O₄ nanoparticles is characterized by a spinel structure, which involves the arrangement of oxygen ions in a cubic close-packed manner while the metal ions occupy both octahedral and tetrahedral sites within the lattice. These nanoparticles also exhibit the catalytic activity, rendering them valuable for catalyzing the chemical reactions. Their small size and high surface area contribute to their effectiveness as catalysts, making them useful in environmental remediation and industrial processes. Their unique composition makes them suitable for applications in catalysis, electronics and energy storage systems [35,36].

Ferrites, particularly magnetic ferrite nanoparticles, have shown promise in efficiently removing heavy metals, dyes, phenols and pharmaceutical residues from wastewater [37-39]. Traditional treatment methods often struggle to efficiently degrade these compounds. Ferrites, however, can play a crucial role in enhancing the degradation of organic pollutants through advanced oxidation processes (AOPs). Ferrite nanoparticles, including Co-NiFe₂O₄ and Cu-ZnFe₂O₄ nanoparticles, hold tremendous promise due to their unique combination of magnetic, electrical and catalytic properties. Their nanoscale dimensions and tunable properties make them suitable for a wide range of applications and extensive research efforts are focused on exploring their potential and optimizing their synthesis methods for desired functionalities. The present work focuses on the development of bimetallic magnetic spinel ferrite Co-NiFe₂O₄ and Cu-ZnFe₂O₄ nanocomposites used for the photodegradation of dyes and wastewater treatment. In particular, the synthesis and characterization methods were explored and the antibacterial activity of the ferrite compounds was tested against *Salmonella typhi*, *Escherichia coli*, *Staphylococcus aureus* and *Bacillus cereus* by well diffusion method.

EXPERIMENTAL

Synthesis: The synthesis of Co-NiFe₂O₄ and Cu-ZnFe₂O₄ spinel ferrite nanoparticles using sol-gel technique was carried out with high grade precursor materials. Firstly, the stoichiometric combinations of cobalt ferrite (CoFe₂O₄), nickel ferrite (NiFe₂O₄), copper ferrite (CuFe₂O₄) and zinc ferrite (ZnFe₂O₄) were dissolved in deionized water to obtain the clear solutions. To maintain the pH and ensure the stability of the solutions, citric acid was added as a chelating agent. The mixtures were then subjected to continuous stirring on a hot plate magnetic

stirrer to achieve the homogeneity and uniform distribution of the ferrite constituents. Following this, the solutions were heated, leading to the formation of gel-like materials as water evaporated. The gels were further heated in an oven at 250 °C for 1 h to convert them into nanopowders. To enhance the structural and magnetic properties of the synthesized bimetallic spinel ferrite nanoparticles, the obtained nanopowders underwent an annealing process at 800 °C for 6 h.

Characterization: The structural integrity of the synthesized bimetallic spinel ferrite nanoparticles Co-NiFe₂O₄ and Cu-ZnFe₂O₄ was determined using an X-ray diffractometer (X-pert Pro, PANalytical B.V., The Netherlands). The main functional groups and chemical bonds of the nanoparticles were observed from FTIR spectroscopy (Perkin-Elmer, USA). The optical stability and configurations were obtained from UV-DRS (Shimadzu-2700, Japan) and the surface modifications were monitored *via* SEM analysis (TITAN, Germany).

RESULTS AND DISCUSSION

XRD studies: Both Co-NiFe₂O₄ and Cu-ZnFe₂O₄ nanoparticles showed unique diffraction peaks at 2θ values of 35.46° and 35.51° (Fig. 1), respectively. These peaks lined up with the spinel crystal structure's (311) plane in the *Fd3m* space group. The JCPDS values for Co-NiFe₂O₄ and Cu-ZnFe₂O₄ were calculated by matching the XRD patterns with the JCPDS database, where Co-NiFe₂O₄ has a JCPDS no. 22-1086, while Cu-ZnFe₂O₄ has JCPDS no. 73-0605. Both nanoparticles have a cubic spinel crystal system in their crystalline nature. The crystal sizes of the Co-NiFe₂O₄ and Cu-ZnFe₂O₄ nanoparticles were determined to be 44.28 and 59.05 nm, respectively. These sizes were calculated using the Scherrer's equation, which utilizes the full width at half maximum (FWHM) of the (311) peak values as listed in Table-1.

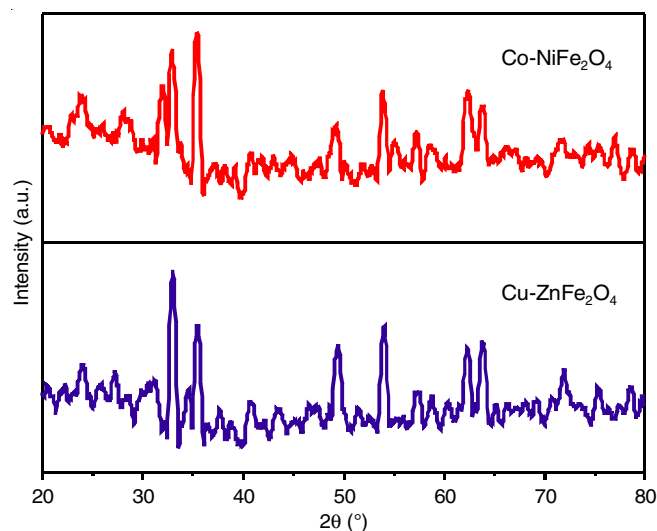


Fig. 1. XRD patterns of Co-Ni Fe₂O₄ and Cu-ZnFe₂O₄ nanoparticles

FTIR spectra: FTIR analysis was performed for the Co-NiFe₂O₄ and Cu-ZnFe₂O₄ samples, which was neatly shown in Fig. 2. For Co-NiFe₂O₄, several characteristic peaks were observed. A peak at 3437 cm⁻¹ indicated the presence of O-H

TABLE-1
XRD PARAMETERS OF Co-Ni Fe₂O₄ AND Cu-ZnFe₂O₄ NANOPARTICLES

Samples	2θ (°)	Height (cts)	FWHM left (2θ,°)	d-spacing (Å)	Crystallite size (nm)
Co-Ni Fe ₂ O ₄	35.4685	131.37	0.1968	2.53096	44.28
Cu-ZnFe ₂ O ₄	35.5132	109.34	0.1476	2.52788	59.05

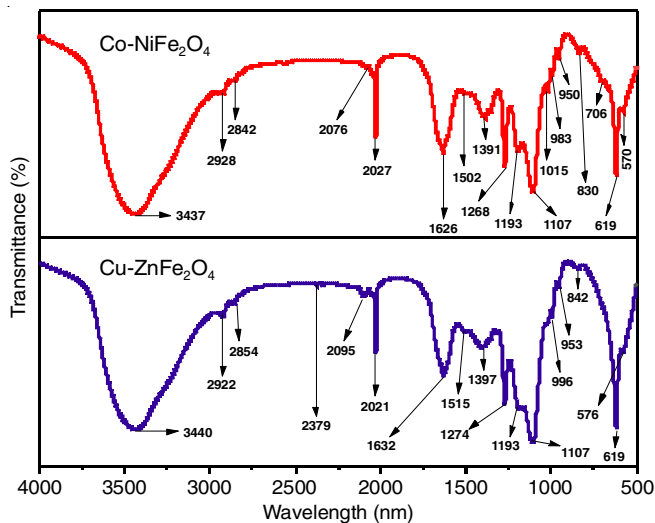


Fig. 2. FTIR spectra of Co-Ni Fe₂O₄ and Cu-ZnFe₂O₄ nanoparticles

stretching vibrations, suggesting the presence of hydroxyl groups or water molecules. Peaks at 2928 and 2842 cm⁻¹ corresponded to the stretching vibrations of CH₂ and CH₃ groups in organic compounds, indicating the presence of organic residues or impurities. The peak at 2076 cm⁻¹ indicated metal-oxygen (M-O) stretching vibrations, confirming the presence of metal-oxide bonds. Another peak at 2027 cm⁻¹ suggested the presence of C≡C stretching vibrations, indicating the presence of alkyne groups or carbon-carbon triple bonds. The presence of C=O stretching vibrations was indicated by the peak at 1626 cm⁻¹, while the peak at 1502 cm⁻¹ corresponded to the aromatic C=C stretching vibrations. Peaks at 1391 cm⁻¹ and 1268 cm⁻¹ represented the metal-oxygen (M-O) bending and C-N stretching vibrations, respectively whereas the peaks at 1193 cm⁻¹, 1107 cm⁻¹, 983 cm⁻¹, 950 cm⁻¹ and 830 cm⁻¹ confirmed the presence of metal-oxygen ν(M-O) stretching and bending vibrations. Finally, the peaks at 706 cm⁻¹, 619 cm⁻¹ and 570 cm⁻¹ indicated the metal-oxygen ν(M-O) stretching and bending vibrations, providing further evidence of metal oxide bonds in the Co-NiFe₂O₄ sample.

For Cu-ZnFe₂O₄, the FTIR analysis revealed the specific peaks as well. A peak at 3440 cm⁻¹ indicated O-H stretching vibrations, suggesting the presence of hydroxyl groups or water molecules. Peaks at 2922 cm⁻¹ and 2854 cm⁻¹ corresponded to the stretching vibrations of CH₂ and CH₃ groups indicating the presence of organic residues or impurities. The peak at 2095 cm⁻¹ represented metal-oxygen ν(M-O) stretching vibrations, confirming the presence of metal oxide bonds, while a peak at 2021 cm⁻¹ suggested C≡C stretching vibrations, indicating the presence of alkyne groups or carbon-carbon triple bonds. The presence of C=O stretching vibrations was indicated by the peak at 1632 cm⁻¹, while the peak at 1515 cm⁻¹ corresponded to

aromatic C=C stretching vibrations. The peaks at 1397 cm⁻¹ and 1274 cm⁻¹ represented the metal-oxygen (M-O) bending and C-N stretching vibrations, respectively, whereas the peaks at 1193 cm⁻¹ and 1107 cm⁻¹ confirmed the presence of metal-oxygen (M-O) stretching vibrations. Also the peaks at 953 cm⁻¹ and 842 cm⁻¹ represented the metal-oxygen (M-O) stretching vibrations, further confirming the presence of metal oxide bonds. Lastly, peaks at 619 cm⁻¹ and 576 cm⁻¹ indicated metal-oxygen (M-O) bending and stretching vibrations, respectively, providing the additional evidence of metal oxide bonds in the Cu-ZnFe₂O₄ sample.

Ultraviolet spectra: The UV analysis results for Co-NiFe₂O₄ nanoparticles at a wavelength of λ = 291 nm revealed the absorbance value of the sample at that specific wavelength as shown in Fig. 3a. The absorbance value indicates the amount of light absorbed by the nanoparticles. The specific value of absorbance at 291 nm for the Co-NiFe₂O₄ nanoparticles would need to be provided to determine the extent of absorption. Similarly, for Cu-ZnFe₂O₄ nanoparticles, the UV analysis results at wavelength of λ = 275 nm indicated the absorbance value for the sample at that particular wavelength (Fig. 3b).

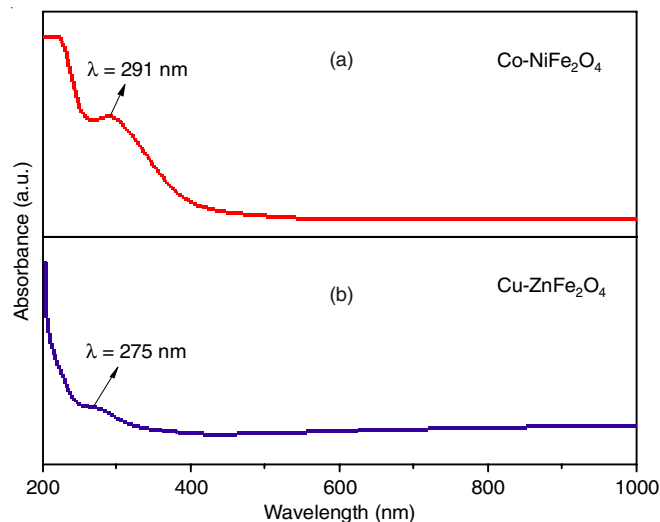


Fig. 3. UV spectra of Co-Ni Fe₂O₄ and Cu-ZnFe₂O₄ nanoparticles

SEM: The microstructure of the Co-doped nickel ferrite and Cu-doped zinc ferrite nanoparticles synthesized *via* the sol-gel method was investigated using scanning electron microscopy (SEM). The calcination temperature influenced the microstructure of the materials, which was observed in the SEM images (Fig. 4). The Co-doped NiFe₂O₄ nanoparticles calcinated at 600 °C had small grains with a diameter of 43 nm compared with Cu-doped ZnFe₂O₄, while Cu-doped ZnFe₂O₄ nanoparticles calcinated at 600 °C had large grains with a diameter of 57 nm. The SEM images showed an agglomerated

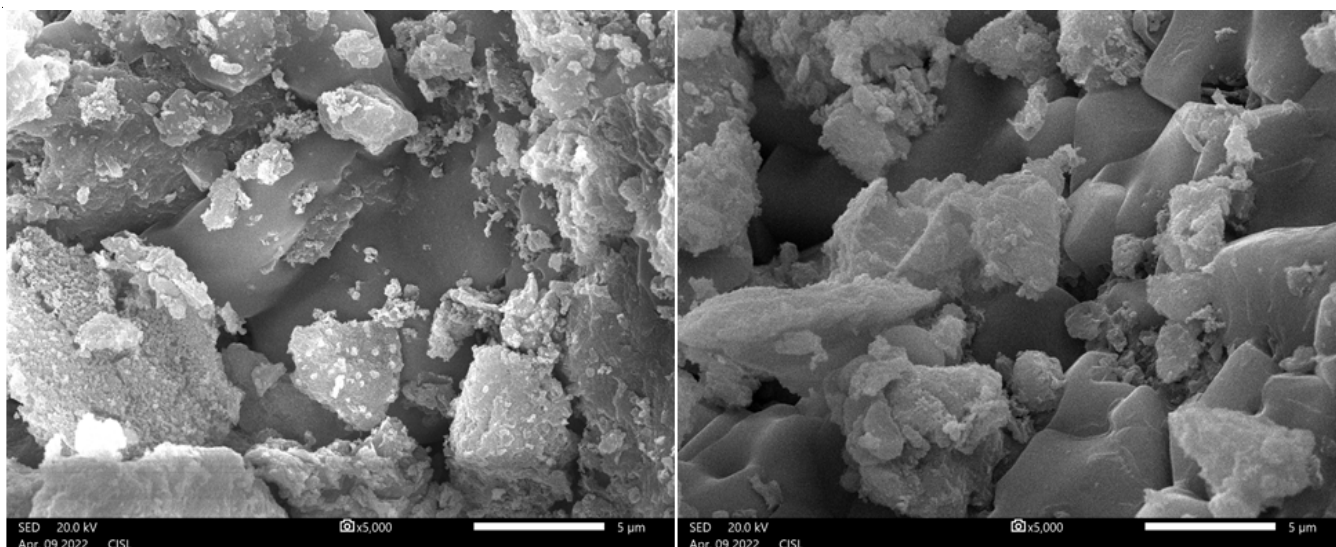


Fig. 4. SEM images of Co-NiFe₂O₄ and Cu-ZnFe₂O₄ nanoparticles

distorted spherical structure in Co-NiFe₂O₄ and a spongy-like structure in Cu-ZnFe₂O₄, which were attributed to the natural interaction between magnetic nanoparticles. The SEM results were in agreement with the XRD results and confirmed the successful synthesis of Co-doped NiFe₂O₄ and Cu-doped ZnFe₂O₄ nanoparticles *via* the sol-gel method.

Vibrating sample magnetometer analysis: The magnetic hysteresis loops of Co-NiFe₂O₄ and Cu-ZnFe₂O₄ nanoparticles exhibit a distinctive S-shaped pattern (Fig. 5), which is the characteristic attribution of the superparamagnetic materials. For Co-doped NiFe₂O₄, coercivity (H_c) was determined as 0.14186 emu, retentivity (M_r) as 52.005 × 10⁻³ emu and saturation magnetization (M_s) as 338.26 Oe. These values demonstrate the impact of Co²⁺ ions on the behaviour of NiFe₂O₄ nanoparticles. Conversely, the Cu-doped ZnFe₂O₄ nanoparticles demonstrated the coercivity (H_c) value of 0.21271 emu, retentivity (M_r) as 71.022 × 10⁻³ emu and saturation magnetization (M_s) as of 285.91 Oe. These evaluations were conducted through a vibrating sample magnetometer at room temperature.

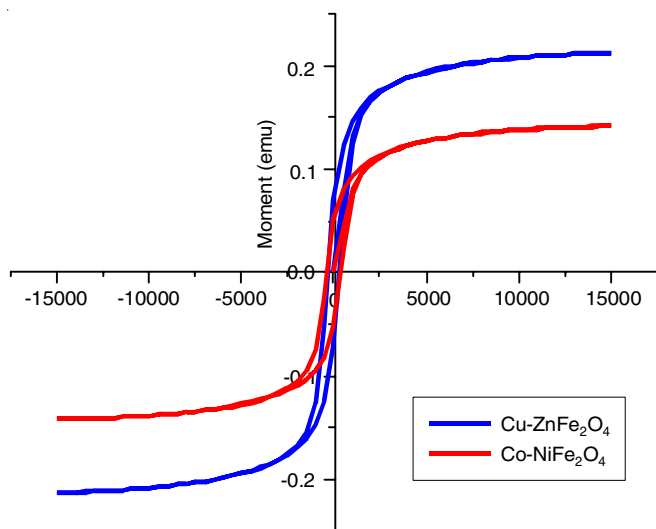


Fig. 5. VSM analysis of Cu-ZnFe₂O₄ and Co-Ni Fe₂O₄ nanoparticles

The outcomes collectively underline the significant role played by the dopant ions (Co²⁺ and Cu²⁺) in shaping the magnetic behaviour of these nanoparticles.

Impact of ferrites on removal of pollutants from the industrial wastewater: Comparing the results in Table-2, it appears that both Co-NiFe₂O₄ and Cu-ZnFe₂O₄ treatments have a similar impact on pH and turbidity, with pH levels being slightly lower after treatment and turbidity remaining relatively consistent. However, there is a slight increase in colour (Harzen units) in both treated glasses of water, with Cu-ZnFe₂O₄ showing the highest increase.

Oil and grease reduction: Both treatments effectively reduced oil and grease levels in the water, with Co-NiFe₂O₄ achieving the lowest concentration at 10.2 mg/L, compared to the raw water value of 12.4 mg/L. In the chlorine reduction, the total residual chlorine levels decreased in both treatments, with Cu-ZnFe₂O₄ achieving the lowest concentration at 2.2 mg/L, lowering from the raw water value of 3.2 mg/L. The qualitative odour remained pungent across all samples indicating that both treatments had no discernible effect on the odour of the treated water. Similarly, the suspended solids showed the minimal changes after treatment, whereas the levels of ammonical nitrogen, total Kjeldahl nitrogen (TKN) and free ammonia were maintained close to those of the raw water.

Biochemical oxygen demand (BOD) levels: Co-NiFe₂O₄ treatment resulted in an increase in BOD to 248 mg/L, while Cu-ZnFe₂O₄ reduced BOD to 188 mg/L, compared to the raw water value of 216 mg/L. These modifications can be interpreted as having various effects on the breakdown of organic materials.

Chemical oxygen demand (COD) levels: There was no difference in the levels of COD between the two treated waters, which indicates that the amounts of organic and inorganic pollutants were comparable.

Heavy metals removal: Both Co-NiFe₂O₄ and Cu-ZnFe₂O₄ nanoparticles are found to be effective in reducing the levels of total arsenic, where Cu-ZnFe₂O₄ achieved the lowest concen-

TABLE-2
EFFECT OF FERRITES REMOVAL OF POLLUTANTS FROM INDUSTRIAL WASTEWATER

Parameter(s)	Unit	Raw water	Co-NiFe ₂ O ₄	Cu-ZnFe ₂ O ₄	General standard for discharge of environmental pollutants Part-A effluents (Schedule-VI) standard limits	
					Inland surface water	Public sewers
pH @ 25 °C	–	7.36	6.28	6.24	5.5-9.0	5.5-9.0
Colour	Hazen	140	150	155	300	–
Turbidity	NTU	6.4	6.4	6.6	–	–
Temperature	°C	25.0	25	25.0	Shall not exceed 5 °C above the receiving water temperature	
Oil & grease	mg/L	12.4	10.2	10.4	10	20
Total residual chlorine	mg/L	3.2	2.4	2.2	1.0	–
Odour	Qualitative	Pungent	Pungent	Pungent	–	–
Suspended solids	mg/L	134.6	136.4	130.6	100	600
Ammoniacal nitrogen as (NH ₃ -N)	mg/L	76.2	76.8	72.4	50	50
Total Kjeldahl nitrogen (TKN) as N	mg/L	138.6	142.4	130.6	100	–
Free ammonia (as NH ₃ -N)	mg/L	18.2	18.2	16.4	5.0	–
BOD (3 days @ 27 °C)	mg/L	216	248	188	30	350
COD	mg/L	2112	2120	1852	250	–
Total arsenic (as As)	mg/L	0.16	0.14	0.10	0.2	0.2
Mercury (as Hg)	mg/L	< 0.01	< 0.01	< 0.01	0.01	0.01
Lead (as Pb)	mg/L	0.06	0.06	0.04	0.1	1.0
Cadmium (as Cd)	mg/L	< 0.005	< 0.005	< 0.005	2.0	1.0
Hexavalent chromium (as Cr ⁶⁺)	mg/L	1.32	1.16	1.08	0.1	2.0
Total chromium (as Cr)	mg/L	2.64	2.18	2.10	2.0	2.0
Copper (as Cu)	mg/L	0.42	0.42	0.32	3.0	3.0
Zinc (as Zn)	mg/L	12.26	12.14	10.26	5.0	15.0
Selenium (as Se)	mg/L	0.06	0.06	0.04	0.05	0.05
Nickel (as Ni)	mg/L	2.78	2.72	2.42	3.0	3.0
Cyanide (as CN)	mg/L	0.12	0.08	0.06	0.2	2.0
Fluoride (as F)	mg/L	4.34	4.36	3.96	2.0	15.0
Dissolved phosphates (as P)	mg/L	7.26	7.82	6.74	5.0	–
Sulphide (as S)	mg/L	0.62	0.64	0.52	2.0	–
Phenolic compounds (as C ₆ H ₅ OH)	mg/L	3.6	3.4	2.8	1.0	5.0
Radioactive materials						
(a) α-Emitters micro curie	mg/L	6 × 10 ⁻⁶	5 × 10 ⁻⁶	4 × 10 ⁻⁶	10 ⁻⁷	10 ⁻⁷
(b) β-Emitters micro curie	mg/L	3 × 10 ⁻⁵	3 × 10 ⁻⁵	2 × 10 ⁻⁵	10 ⁻⁶	10 ⁻⁶
Bio-assay test	–	0% Survival of fish after 96 h	0% Survival of fish after 96 h	0% Survival of fish after 96 h	Minimum 90% survival of fish after 96 h with 90% effluent and 10% dilution water	
Manganese (as Mn)	mg/L	0.012	0.010	0.008	2.0	2.0
Iron (as Fe)	mg/L	3.34	3.24	3.04	3.0	3.0
Vanadium (as V)	mg/L	< 0.05	< 0.05	< 0.05	0.2	0.2
Nitrate (as NO ₃)	mg/L	42.4	39.2	36.4	10	–
Total Hardness (as CaCO ₃)	mg/L	464	530	404	–	–
Calcium (as Ca)	mg/L	116	132	102	–	–
Magnesium (as Mg)	mg/L	42	48	36	–	–
Total alkalinity (as CaCO ₃)	mg/L	564	542	492	–	–
Chlorides (as Cl)	mg/L	420	406	350	600	–
Total dissolved solids	mg/L	1924	2216	1394	1500	–
Sulphate (as SO ₄)	mg/L	316	292	216	400	–
Dissolved oxygen	mg/L	1.8	2.2	2.8	4.0	–
Pesticides	µg/L	36.4	22.6	22.6	–	–
Pigment content	mg/L	5.2	4.4	4.2	–	–
Dye content	mg/L	2.8	2.2	2.2	–	–

Note: BOD = Biochemical oxygen demand, COD = Chemical oxygen demand, Hyphen (–) denotes limits not provided by PCB. As per the above analyzed Schedule-VI Discharge standard parameters for inland surface water quality was deviated from the standards, so this water is contaminated and polluted due to the interference of the nearest domestic/commercial/industrial effluents and wastewater.

tration at 0.10 mg/L. Mercury and cadmium levels were below the detection limit in all the samples indicating the effective removal of these heavy metals.

Again both Co-NiFe₂O₄ and Cu-ZnFe₂O₄ nanoparticles effectively reduced hexavalent chromium (Cr⁶⁺) and total Cr concentrations, with Cu-ZnFe₂O₄ achieving the lowest levels.

Copper levels remained similar, while Cu-ZnFe₂O₄ led to a reduction in zinc concentration. Selenium concentrations were maintained and Cu-ZnFe₂O₄ resulted in a decrease in nickel concentration. Both treatments effectively reduced cyanide levels also, with Cu-ZnFe₂O₄ achieving the lowest concentration. The addition of Co-NiFe₂O₄ resulted in an increase in the concentration of dissolved phosphates, whereas Cu-ZnFe₂O₄ led to a reduction of phosphorus. However, both treatments had a negligible effect on the concentration of sulphides. Other parameters, including phenolic compounds, radioactive materials, manganese, iron, vanadium, nitrate, total hardness and calcium, generally showed improvements or maintained levels similar to raw water.

In summary, both Co-NiFe₂O₄ and Cu-ZnFe₂O₄ treatments demonstrated effectiveness in altering the water quality parameters, with variations in their impact on certain parameters like colour and BOD. The choice between these treatments should consider the specific goals of industrial wastewater treatment and the trade-offs involved in pH adjustment, colour removal and organic matter degradation. Additionally, the treatments effectively removed heavy metals and reduced chlorine levels, contributing to improved water quality. Co-NiFe₂O₄ treatment led to increased magnesium levels and total dissolved solids, while Cu-ZnFe₂O₄ resulted in lower levels of chloride, sulfate and total dissolved solids. Both treatments improved the dissolved oxygen levels and effectively reduced pesticide, pigment and dye concentrations. The results highlight the efficacy of Co-NiFe₂O₄ and Cu-ZnFe₂O₄ nanomaterials in addressing certain pollutants while maintaining or simply modifying other water quality factors, stressing their potential for comprehensive treatment of industrial wastewater.

Antibacterial activity of ferrite nanoparticles: *In vitro* antimicrobial activity of bimetallic spinel ferrite nanoparticles suspensions of different concentrations (2.5, 5, 7.5, 10 µg/µL and control) towards various bacterial pathogens (Gram-positive and Gram-negative) were tested by well-diffusion method. It was found that increasing concentrations of bimetallic spinel ferrite nanoparticles had a significant bactericidal activity against bacterial strains (Fig. 6). The bimetallic spinel ferrite nanoparticles showed the antimicrobial activity against selected pathogens such as *Staphylococcus aureus* (ATCC 25923), *Bacillus cereus* (ATCC 27853), *Escherichia coli* (ATCC 8739) and *Salmonella typhimurium* (ATCC 14028). The maximum zone of inhibition were observed in *S. aureus* (28 mm), *B. cereus* (10 mm), *E. coli* (12 mm) and *S. typhimurium* (10 mm). There are several possible mechanisms for the antibacterial action of zinc ion. It has been suggested that zinc bind to the membranes of microorganisms, similar to mammalian cell. This result agreed with previous report, that bimetallic spinel ferrite nanoparticles may disperse and damage bacterial cell membrane, resulting in a leakage of intracellular fluid and loss of osmotic pressure [40].

Conclusion

In summary, the Co-doped nickel ferrite and Cu-doped zinc ferrite nanoparticles were successfully synthesized through the sol-gel method, the XRD analysis confirmed the formation

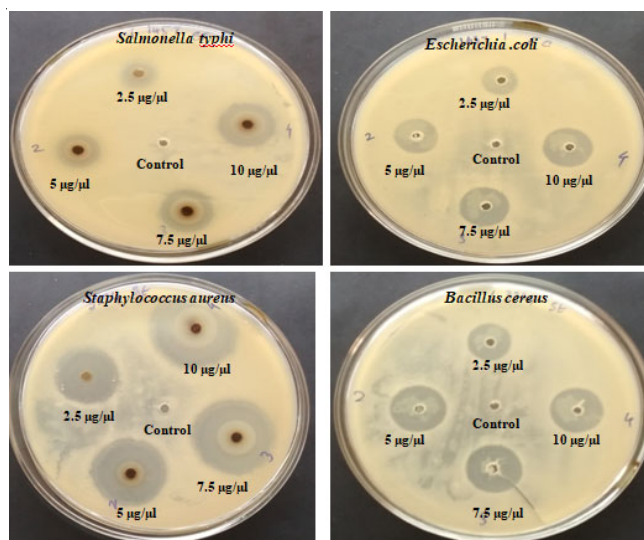


Fig. 6. Antibacterial activity of ferrite nanoparticles

of spinel structures for both nanomaterials. The FTIR and UV analysis shed light on the chemical composition, molecular vibrations and absorption properties of the Co-NiFe₂O₄ and Cu-ZnFe₂O₄ nanoparticles. The SEM images revealed that the calcination temperature influenced the microstructure of the materials, with Co-NiFe₂O₄ displaying an agglomerated distorted spherical structure and Cu-ZnFe₂O₄ exhibiting a spongy-like structure. The magnetic properties of the samples were also characterized and the results showed a clear impact of Co²⁺ and Cu²⁺ ions on the magnetic behaviour of the bimetallic spinel ferrite nanoparticles, with the S-shaped hysteresis loop indicating the super paramagnetic properties. It has good antibacterial potential against both Gram-positive and Gram-negative bacteria and efficiently kill or inhibit the growth of bacteria from the polluted water. The water treatments with Co-NiFe₂O₄ and Cu-ZnFe₂O₄ nanomaterials have shown their effectiveness in modifying a wide range of water quality parameters. These treatments successfully reduced concentrations of various contaminants including heavy metals, pesticides and organic compounds, while also altering parameters like alkalinity, chloride levels and total dissolved solids. Moreover, both treatments improved dissolved oxygen levels in the treated water. The results highlight the potential of Co-NiFe₂O₄ and Cu-ZnFe₂O₄ materials for specific and extensive treatment of industrial wastewater. The choice between them depends on individual treatment objectives and the desired effect on water quality indices.

CONFLICT OF INTEREST

The authors declare that there is no conflict of interests regarding the publication of this article.

REFERENCES

- G. Rana, P. Dhiman, A. Kumar, D.V. Vo, G. Sharma, S. Sharma and M. Naushad, *Chem. Eng. Res. Des.*, **175**, 182 (2021); <https://doi.org/10.1016/j.cherd.2021.08.040>
- S. Jauhar, J. Kaur, A. Goyal and S. Singhal, *RSC Adv.*, **6**, 97694 (2016); <https://doi.org/10.1039/C6RA21224G>

3. P.A. Vinosha, A. Manikandan, A.S. Judith Ceicilia, A. Dinesh, G. Francisco-Nirmala, A.C. Preetha, Y. Slimani, M.A. Almessiere, A. Baykal and B. Xavier, *Ceram. Int.*, **47**, 10512 (2021); <https://doi.org/10.1016/j.ceramint.2020.12.289>
4. Y. Bhattacharjee and S. Bose, *ACS Appl. Nano Mater.*, **4**, 949 (2021); <https://doi.org/10.1021/acsanm.1c00278>
5. J. Philip and J.M. Laskar, *J. Nanofluids*, **1**, 3 (2012); <https://doi.org/10.1166/jon.2012.1002>
6. M.B. Gawande, A. Goswami, T. Asefa, H. Guo, A.V. Biradar, D.L. Peng, R. Zboril and R.S. Varma, *Chem. Soc. Rev.*, **44**, 7540 (2015); <https://doi.org/10.1039/C5CS00343A>
7. S. Kalia, S. Kango, A. Kumar, Y. Haldorai, B. Kumari and R. Kumar, *Colloid Polym. Sci.*, **292**, 2025 (2014); <https://doi.org/10.1007/s00396-014-3357-y>
8. H. Osgood, S.V. Devaguptapu, H. Xu, J. Cho and G. Wu, *Nano Today*, **11**, 601 (2016); <https://doi.org/10.1016/j.nantod.2016.09.001>
9. H. Qin, Y. He, P. Xu, D. Huang, Z. Wang, H. Wang, Z. Wang, Y. Zhao, Q. Tian and C. Wang, *Adv. Colloid Interface Sci.*, **294**, 102486 (2021); <https://doi.org/10.1016/j.cis.2021.102486>
10. W. Hu, S. Chen, J. Yang, Z. Li and H. Wang, *Carbohydr. Polym.*, **101**, 1043 (2014); <https://doi.org/10.1016/j.carbpol.2013.09.102>
11. J. Wu, S. Li and H. Wei, *Nanoscale Horiz.*, **3**, 367 (2018); <https://doi.org/10.1039/C8NH00070K>
12. K.K. Kefeni, T.A.M. Msagati and B.B. Mamba, *Mater. Sci. Eng. B*, **215**, 37 (2017); <https://doi.org/10.1016/j.mseb.2016.11.002>
13. G. Chen, I. Roy, C. Yang and P.N. Prasad, *Chem. Rev.*, **116**, 2826 (2016); <https://doi.org/10.1021/acs.chemrev.5b00148>
14. A. Ali, T. Shah, R. Ullah, P. Zhou, M. Guo, M. Ovais, Z. Tan and Y.K. Rui, *Front. Chem.*, **9**, 629054 (2021); <https://doi.org/10.3389/fchem.2021.629054>
15. W. Wu, Q. He and C. Jiang, *Nanoscale Res. Lett.*, **3**, 397 (2008); <https://doi.org/10.1007/s11671-008-9174-9>
16. B. Issa, I.M. Obaidat, B.A. Albiss and Y. Haik, *Int. J. Mol. Sci.*, **14**, 21266 (2013); <https://doi.org/10.3390/ijms141121266>
17. E. Ye, M.D. Regulacio, S.Y. Zhang, X.J. Loh and M.Y. Han, *Chem. Soc. Rev.*, **44**, 6001 (2015); <https://doi.org/10.1039/C5CS00213C>
18. S. Jung, W. Cho, H.J. Lee and M. Oh, *Angew. Chem.*, **121**, 1487 (2009); <https://doi.org/10.1002/ange.200804816>
19. G.J. Owens, R.K. Singh, F. Foroutan, M. Alqaysi, C.M. Han, C. Mahapatra, H.W. Kim and J.C. Knowles, *Prog. Mater. Sci.*, **77**, 1 (2016); <https://doi.org/10.1016/j.pmatsci.2015.12.001>
20. C. Ching Lau, M. Kemal Bayazit, P.J. Reardon and J. Tang, *Chem. Rec.*, **19**, 172 (2019); <https://doi.org/10.1002/tcr.201800121>
21. W. Ren, G. Lin, C. Clarke, J. Zhou and D. Jin, *Adv. Mater.*, **32**, 1901430 (2020); <https://doi.org/10.1002/adma.201901430>
22. J.K. Sharma, P. Srivastava, G. Singh and H.S. Virk, Nanoferrites of Transition Metals and their Catalytic Activity, In: Solid State Phenomena Trans Tech Publications Ltd., vol. 241, pp. 126-138 (2016).
23. S. Kalia, A. Kumar, S. Sharma and N. Prasad, *J. Phys.: Conf. Ser.*, **2267**, 012133 (2022); <https://doi.org/10.1088/1742-6596/2267/1/012133>
24. J. Kwon, J.H. Kim, S.H. Kang, C.J. Choi, J.A. Rajesh and K.S. Ahn, *Appl. Surf. Sci.*, **413**, 83 (2017); <https://doi.org/10.1016/j.apsusc.2017.04.022>
25. M.G. Naseri, E.B. Saion and A. Kamali, *Int. Schol. Res. Notices*, **2012**, 604241 (2012); <https://doi.org/10.5402/2012/604241>
26. K. Hantanasirisakul and Y. Gogotsi, *Adv. Mater.*, **30**, 1804779 (2018); <https://doi.org/10.1002/adma.201804779>
27. B. Shao, Z. Liu, G. Zeng, H. Wang, Q. Liang, Q. He, M. Cheng, C. Zhou, L. Jiang and B. Song, *J. Mater. Chem. A Mater. Energy Sustain.*, **8**, 7508 (2020); <https://doi.org/10.1039/D0TA01552K>
28. B. Dieny and M. Chshiev, *Rev. Mod. Phys.*, **89**, 025008 (2017); <https://doi.org/10.1103/RevModPhys.89.025008>
29. A. Tyagi, S. Banerjee, J. Cherusseri and K.K. Kar, Characteristics of transition metal oxides. Handbook of Nanocomposite Supercapacitor Materials I: Characteristics, Springer, pp. 91-123 (2020).
30. G.K. Prasad, J.P. Kumar, L.K. Pandey and B. Singh, *Adv. Porous Mater.*, **5**, 1 (2017); <https://doi.org/10.1166/apm.2017.1132>
31. S.J. Salih and W.M. Mahmood, *Heliyon*, **9**, e16601 (2023); <https://doi.org/10.1016/j.heliyon.2023.e16601>
32. M. Zheng, Z.S. Wang, J.Q. Wu and Q. Wang, *J. Nanopart. Res.*, **12**, 2211 (2010); <https://doi.org/10.1007/s11051-009-9787-7>
33. A. Lavin, R. Sivasamy, E. Mosquera and M.J. Morel, *Surf. Interfaces*, **17**, 100367 (2019); <https://doi.org/10.1016/j.surfin.2019.100367>
34. A. Mahmoud, M. Echabaane, K. Omri, L. El Mir and R. Ben Chaabane, *J. Alloys Compd.*, **786**, 960 (2019); <https://doi.org/10.1016/j.jallcom.2019.02.060>
35. K. Malaie and M.R. Ganjali, *J. Energy Storage*, **33**, 102097 (2021); <https://doi.org/10.1016/j.est.2020.102097>
36. C. Pereira, R.S. Costa, L. Lopes, B. Bachiller-Baeza, I. Rodríguez-Ramos, A. Guerrero-Ruiz, P.B. Tavares, C. Freire and A.M. Pereira, *Nanoscale*, **10**, 12820 (2018); <https://doi.org/10.1039/C8NR03533D>
37. A.B. Mapossa, W. Mhike, J.L. Adalima and S. Tichapondwa, *Catalysts*, **11**, 1543 (2021); <https://doi.org/10.3390/catal11121543>
38. K.K. Kefeni, B.B. Mamba, T.A.M. Msagati, *Sep. Purif. Technol.*, **188**, 399 (2017); <https://doi.org/10.1016/j.seppur.2017.07.015>
39. D.M. Tejashwini, H.V. Harini, H.P. Nagaswarupa, R. Naik, S. Harlapur and N. Basavaraju, *Results Chem.*, **7**, 101247 (2024); <https://doi.org/10.1016/j.rechem.2023.101247>
40. Y. Liu, L. He, A. Mustapha, H. Li, Z.Q. Hu and M. Lin, *J. Appl. Microbiol.*, **107**, 1193 (2009); <https://doi.org/10.1111/j.1365-2672.2009.04303.x>